Ballistic transport in disordered graphene

A. Schuessler[*], P. M. Ostrovsky[*,†], I. V. Gornyi[*,**] and A. D. Mirlin[*,§]

[*]*Institut für Nanotechnologie, Forschungszentrum Karlsruhe, 76021 Karlsruhe, Germany*
[†]*L. D. Landau Institute for Theoretical Physics RAS, 119334 Moscow, Russia*
[**]*A.F. Ioffe Physico-Technical Institute, 194021 St. Petersburg, Russia*
[‡]*Inst. für Theorie der kondensierten Materie, Universität Karlsruhe, 76128 Karlsruhe, Germany*
[§]*Petersburg Nuclear Physics Institute, 188300 St. Petersburg, Russia*

Abstract. An analytic theory of electron transport in disordered graphene in a ballistic geometry is developed. We consider a sample of a large width W and analyze the evolution of the conductance, the shot noise, and the full statistics of the charge transfer with increasing length L, both at the Dirac point and at a finite gate voltage. The transfer matrix approach combined with the disorder perturbation theory and the renormalization group is used. We also discuss the crossover to the diffusive regime and construct a "phase diagram" of various transport regimes in graphene.

PACS: 73.63.-b, 73.22.-f

1. INTRODUCTION

Recent successes in manufacturing of atomically thin graphite samples [1, 2, 3, 4] (graphene) have stimulated intense experimental and theoretical activity [5, 6]. The key feature of graphene is the massless Dirac type of low-energy electron excitations. This gives rise to a number of remarkable physical properties of this system distinguishing it from conventional two-dimensional metals. One of the most prominent features of graphene is the "minimal conductivity" at the neutrality (Dirac) point. Specifically, the conductivity [3, 4, 7] of an undoped sample is close to e^2/h per spin per valley, remaining almost constant in a very broad temperature range — from room temperature down to 30mK.

A number of numerical simulations of electron transport in disordered graphene [8, 9, 10, 11, 12, 13, 14] confirmed the absence of localization in the presence of long-range random potential. The main quantity studied numerically in most of these works is the conductance G of a finite-size graphene sample with a width W much larger than the length L. This setup allows one to define the "conductivity" $\sigma \equiv GL/W$ even for ballistic samples with L much shorter than the mean free path l. Remarkably, in graphene at the Dirac point, such ballistic "conductivity" has a universal value $e^2/\pi h$ in the clean case [15, 16]. This setup was studied experimentally in Refs. [17, 18, 19, 20] and the ballistic value $e^2/\pi h$ was indeed observed for large aspect ratios. This geometry of samples is particularly advantageous for the analysis of evolution from the ballistic to diffusive transport.

A complete description of the electron transport through a finite system involves not only the conductance but also higher cumulants of the distribution of transferred charge. The second moment is related to the current noise in the system. The intensity of the shot noise is characterized by the Fano factor F. For clean graphene, this quantity was studied in Ref. [16]. Surprisingly, in a short and wide sample ($W \gg L$) the Fano factor takes the universal value $F = 1/3$, that coincides with the well-known result for a diffusive metallic wire [21]. This is at odds with usual clean metallic systems, where the shot noise is absent ($F = 0$). The Fano factor $F = 1/3$ in clean graphene is attributed [16] to the fact that the current is mediated by evanescent rather than propagating modes. Furthermore, the whole distribution of transmission eigenvalues for the massless Dirac equation in a clean sample at the Dirac point agrees with that of mesoscopic metallic wires in the diffusive regime [22].

The effect of disorder on the shot noise was studied numerically in Refs. [12, 13], where the value of the Fano factor $F \approx 0.3$ was found across the whole crossover form ballistics to diffusion. The Fano factor close to $1/3$ was also observed at the Dirac point experimentally [19, 20]. When the chemical potential was shifted away from the Dirac point, the Fano factor decreased, then showed an intermediate shoulder at $F \approx 0.15$, and finally approached zero for largest gate voltages (carrier concentrations).

While both diffusive and clean limits have been addressed analytically, only numerical and experimental results for the intermediate regime of ballistic transport through disordered samples have been available so far [23]. The aim of this paper is to fill this gap. We develop the analytic theory of electron transport in disordered graphene in the ballistic geometry ($L \ll W, l$) and calculate the full statistics of the charge transfer for both zero (the Dirac point) and large concentration of carriers. We also discuss the crossover to diffusive regime and construct the overall "phase diagram" of transport

regimes.

A number of experimental results show that the dominant disorder in graphene scatters electrons within the same valley. First, this disorder model is supported by the odd-integer quantization [3, 4, 5] of the Hall conductivity, $\sigma_{xy} = (2n+1)2e^2/h$, representing a direct evidence [24] in favor of smooth disorder which does not mix the valleys. The analysis of weak localization also corroborates the dominance of intra-valley scattering [25]. Furthermore, the observation of the linear density dependence [5] of graphene conductivity away from the Dirac point implies that the relevant disorder is due to charged impurities and/or ripples [8, 26, 27, 28, 29], that is a particular type of long-range disorder. Finally, apparent absence of localization at the Dirac point down to very low temperatures [3, 4, 7] can be explained only by some special symmetry of disorder. In particular, a lack of valley mixing leads to emergence of a topological term in the corresponding field theory (unitary or symplectic σ-model) [30]. The peculiar topological properties protect the system from localization [30, 31, 24, 32, 11]. It is worth mentioning that a topologically protected metallic state emerging in graphene with long-range random potential also arises at a surface of a three-dimensional Z_2 topological insulator [33, 34].

Motivated by the experimental observations, we will adopt the single-valley model of graphene. More specifically, we will consider potential disorder that scatters within a single valley and neglect intervalley scattering events. A more general study allowing for other intravalley scattering mechanisms (random vector potential and random Dirac mass) can be found in Ref. [35].

2. TRANSFER-MATRIX TECHNIQUE

We start with introducing our model and the general formalism of transfer matrix technique. For graphene, this approach was employed in Refs. [15, 16, 36, 37, 38, 12].

The single-valley massless Dirac Hamiltonian of electrons in graphene has the form (see, e.g., Ref. [6])

$$H = v_0 \boldsymbol{\sigma}\mathbf{p} + V(x,y). \qquad (1)$$

Here $\boldsymbol{\sigma} \equiv \{\sigma_x, \sigma_y\}$ is the two-dimensional vector of Pauli matrices acting on the electron pseudospin degree of freedom corresponding to the sublattice structure of the honeycomb lattice and the Fermi velocity is $v_0 \approx 10^8$ cm/s. The random part $V(x,y)$ is in general a 2×2 matrix in the sublattice space. We will consider only the case of potential disorder, when the operator $V(x,y)$ is trivial in the pseudospin space. For a more general case see Ref. [35]. Below we set $\hbar = 1$ and $v_0 = 1$ for convenience.

We will calculate transport properties of a rectangular graphene sample with the dimensions $L \times W$. The contacts are attached to the two sides of the width W separated by the distance L. We fix the x axis in the direction of current, Fig. 1, with the contacts placed at $x = 0$ and $x = L$. We assume $W \gg L$, which allows us to neglect the boundary effects related to the edges of the sample that are parallel to the x axis (at $y = \pm W/2$).

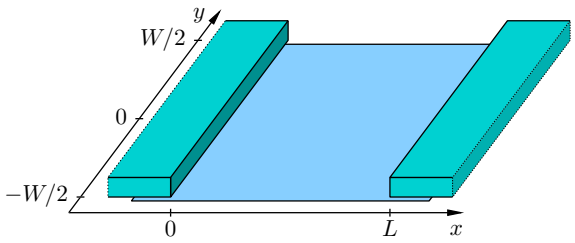

FIGURE 1. Schematic setup for two-terminal transport measurements. Graphene sample of dimensions $L \times W$ is placed between two parallel contacts. We assume $W \gg L$ throughout the paper.

Following Ref. [16], metallic contacts are modelled as highly doped graphene regions described by the same Hamiltonian (1). In other words, we assume that the chemical potential E_F in the contacts is shifted far from the Dirac point. In particular, $E_F \gg \varepsilon$, where ε is the chemical potential inside the graphene sample counted from the Dirac point. (All our results are independent of the sign of energy, thus we assume $\varepsilon > 0$ throughout the paper.) A large number of propagating modes exists in the leads, all belonging to the circular Fermi surface of radius $p_F = E_F/v_0$. These modes are labelled by the momentum $p_n = 2\pi n/W$ in y direction with $|n| < N = W p_F/2\pi$. Particular boundary conditions at $y = \pm W/2$ shift the quantized values of p_n by a constant of order $1/W$. However, this constant has no significance in the limit $W \gg L$ when many channels participate in electron transport.

We will use the mixed momentum-coordinate representation, with the wave function $\Psi_n(x)$ bearing a vector index n in the space of transverse momenta supplemented by a 2-spinor structure in pseudospin (sublattice) space. The eigenstates of the clean Hamiltonian $H_0 = v_0 \boldsymbol{\sigma}\mathbf{p}$ have the direction of pseudospin parallel to the electron momentum. It is convenient to perform the unitary rotation [38] in the pseudospin space $\psi = \mathscr{L}\Psi$ with $\mathscr{L} = (\sigma_x + \sigma_z)/\sqrt{2}$ which transforms σ_x to the diagonal form: $\mathscr{L}\sigma_x\mathscr{L}^\dagger = \sigma_z$. Hence the two components of the rotated spinor correspond to right- and left-propagating waves, $\psi = \{\psi^R, \psi^L\}$. In terms of the new function $\psi_n(x)$, the Schrödinger equation $H\Psi = \varepsilon\Psi$ acquires the form [12, 38]

$$\frac{\partial \psi_n}{\partial x} = (\sigma_x p_n + i\sigma_z \varepsilon)\psi_n - i\sigma_z \sum_m U_{nm}(x)\psi_m. \qquad (2)$$

The matrix $U_{nm}(x)$ represents the operator $V(x,y)$ in the mixed momentum-coordinate representation

$$U_{nm}(x) = \int \frac{dy}{W}\, e^{-i(p_n - p_m)y} V(x,y). \qquad (3)$$

A standard description of electron propagation involves the transfer matrix $\mathscr{T}$ which relates left- and right-moving waves at the point $x = L$ to those at $x = 0$:

$$\begin{pmatrix} \psi^R(L) \\ \psi^L(L) \end{pmatrix} = \mathscr{T} \begin{pmatrix} \psi^R(0) \\ \psi^L(0) \end{pmatrix}, \quad \mathscr{T} = \begin{pmatrix} t^{\dagger -1} & r t^{-1} \\ -t^{-1} r & t^{-1} \end{pmatrix}. \qquad (4)$$

The elements t and r are matrices in channel space formed by transmission and reflection amplitudes respectively. This description is convenient due to the simple multiplicativity property: $\mathscr{T}(x_3,x_2)\mathscr{T}(x_2,x_1) = \mathscr{T}(x_3,x_1)$.

By definition, the transfer matrix $\mathscr{T}(x_2,x_1)$ yields a solution to the Schrödinger equation (2) in the form $\psi(x_2) = \mathscr{T}(x_2,x_1)\psi(x_1)$. Transfer matrix itself, as a function of its first argument, obeys the same Schrödinger equation with the initial condition $\mathscr{T}(x,x) = \mathbb{1}$. In a clean sample the solution depends only on the difference $x_2 - x_1$ and is diagonal in channel space:

$$\mathscr{T}^{(0)}_{nm}(x_2,x_1) = \delta_{nm} \exp\left[(\sigma_x p_n + i\sigma_z \varepsilon)(x_2 - x_1)\right]. \qquad (5)$$

In order to include disorder as a perturbation, it is convenient to cast the Schrödinger equation (2) into an integral form. In terms of transfer matrix the integral equation reads

$$\mathscr{T}(x_2,x_1) = \mathscr{T}^{(0)}(x_2,x_1) - i\int_{x_1}^{x_2} dx\, \mathscr{T}^{(0)}(x_2,x)\sigma_z U(x) \mathscr{T}(x,x_1). \qquad (6)$$

The transport statistics of the sample is expressed in terms of transmission eigenvalues T_n — the eigenvalues of the matrix $t^\dagger t$. One can extract these transmission eigenvalues from the upper left element of the transfer matrix (4). The first two moments of the transferred charge distribution determine the conductance (by Landauer formula) and the Fano factor [21]

$$G = \frac{4e^2}{h}\,\mathrm{Tr}(t^\dagger t), \qquad F = 1 - \frac{\mathrm{Tr}(t^\dagger t)^2}{\mathrm{Tr}(t^\dagger t)}. \qquad (7)$$

The factor 4 in the expression for the conductance accounts for the spin and valley degeneracy.

3. CLEAN GRAPHENE

We will first analyze transport properties of a clean graphene strip. In the "short and wide" geometry ($W \gg L$) we are considering, the total number of channels participating in charge transfer is large. This allows us to replace summation over channels by integration. From now on, we will identify channels by the dimensionless momentum $p = p_n L$ in y direction.

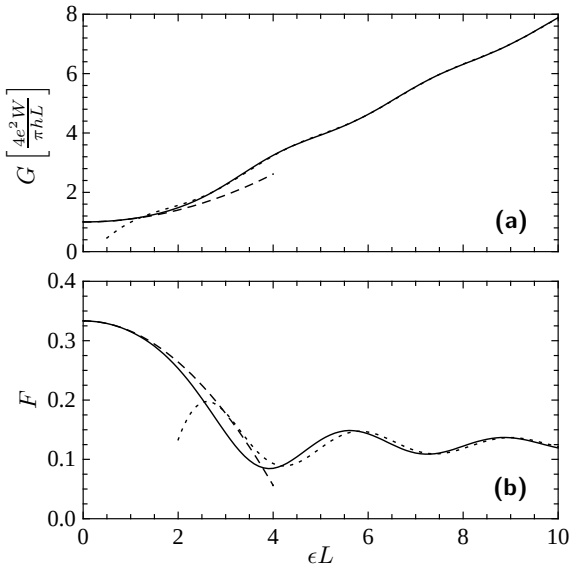

FIGURE 2. Energy dependence of the (a) conductance and the (b) Fano factor of the clean sample with $W \gg L$. Solid lines show numerical results. Low energy asymptotics Eq. (12) is plotted by dashed lines while dotted lines correspond to high energy limit Eqs. (19) and (20). Asymptotical curves provide a very good approximation to the exact result in the whole range of energies.

The transfer matrix $\mathscr{T}^{(0)}$, and hence its upper-left block $t^{\dagger -1}$, are diagonal in channels. Using the explicit form of the clean graphene transfer matrix, Eq. (5), one calculates the transmission eigenvalues [38]

$$T_p = (t^\dagger t)_{pp} = \left[1 + \frac{p^2 \sinh^2 \sqrt{p^2 - (\varepsilon L)^2}}{p^2 - (\varepsilon L)^2}\right]^{-1}. \qquad (8)$$

For the conductance and Fano factor we obtain from Eq. (7)

$$G = \frac{2e^2 W}{\pi h L} \int dp\, T_p, \qquad F = 1 - \frac{\int dp\, T_p^2}{\int dp\, T_p}. \qquad (9)$$

The result of numerical integration of Eq. (9) is shown in Fig. 2. A detailed analytical analysis of the two limiting cases of small and large energies is presented below.

3.1. Low energies: $\varepsilon L \ll 1$

In the limit of low energies, $\varepsilon L \ll 1$, we describe transport properties with the help of a distribution function

$P(T)$ of transmission eigenvalues (8). This distribution function provides a measure in the space of channels,

$$P(T)\,dT = \frac{W\,d|p|}{\pi L}. \tag{10}$$

According to (8), there is one-to-one correspondence between the transmission eigenvalue $0 \le T \le 1$ and the absolute value $|p|$ of the momentum; an extra factor of 2 in the right-hand side of Eq. (10) accounts for the double degeneracy between channels with momenta p and $-p$.

In the low energy limit, we calculate the distribution function $P(T)$ in the form of a power series in the small parameter εL. In order to perform this calculation, we invert the function T_p given by Eq. (8) keeping terms of the second order in εL and then substitute the result into Eq. (10).

$$P(T) = \frac{W}{2\pi L}\frac{1}{T\sqrt{1-T}} \times \left[1 + (\varepsilon L)^2\left(\frac{\sqrt{1-T}}{\operatorname{arccosh}^3\frac{1}{\sqrt{T}}} - \frac{1+T}{2\operatorname{arccosh}^2\frac{1}{\sqrt{T}}}\right)\right]. \tag{11}$$

At zero energy, the function $P(T)$ reproduces the well-known Dorokhov result [39] for a diffusive wire. This is, in particular, the reason for the $1/3$ Fano factor in graphene [16]. The fact that the clean graphene sample is characterized by exactly the same form of the transmission distribution as a generic diffusive wire is highly nontrivial. We will show below (Secs. 4 and 5) that this remarkable correspondence remains valid in the ballistic regime when leading disorder effects are incorporated.

Using the distribution (11), we obtain the following results for the conductance and the Fano factor of clean graphene at low energies, $\varepsilon L \ll 1$,

$$G = \frac{4e^2}{\pi h}\,\frac{W}{L}\left[1 + c_1(\varepsilon L)^2\right], \quad F = \frac{1}{3}\left[1 + c_2(\varepsilon L)^2\right], \tag{12}$$

$$c_1 = \frac{35\zeta(3)}{3\pi^2} - \frac{124\zeta(5)}{\pi^4} \approx 0.101, \tag{13}$$

$$c_2 = -\frac{28\zeta(3)}{15\pi^2} - \frac{434\zeta(5)}{\pi^4} + \frac{4572\zeta(7)}{\pi^6} \approx -0.052. \tag{14}$$

At the Dirac point ($\varepsilon = 0$), Eq. (12) reproduces the earlier analytical results of Refs. [15, 16]. Low energy asymptotics is shown with dashed lines in Fig. 2.

3.2. High energies: $\varepsilon L \gg 1$

When the Fermi energy ε in the sample is far from the Dirac point, many conducting ($T \sim 1$) channels are opened. In this regime, the conductivity and higher moments of the transmission distribution are essentially linear in ε with small oscillating corrections (see Fig. 2). These oscillations are due to interference effects: conductance is relatively enhanced and the noise is suppressed when a channel exhibits resonant transmission with T close to 1. This phenomenon is similar to the Fabry-Perot resonances.

At high energies, it is convenient to deal with the generating function of transmission moments defined as

$$\mathscr{F}(z) = \sum_{n=1}^{\infty} z^{n-1}\,\mathrm{Tr}(t^\dagger t)^n = \mathrm{Tr}\left[t^{-1}t^{\dagger\,-1} - z\right]^{-1}. \tag{15}$$

In order to calculate $\mathscr{F}(z)$, we substitute Eq. (8) into Eq. (15). The integrand oscillates rapidly in the interval $-\varepsilon L < p < \varepsilon L$. This interval of momenta contains all open (well-conducting) channels and thus provides the main contribution to the generating function. We introduce a new variable u, such that $p = \varepsilon L\sqrt{1-u^2}$. In terms of this new variable the integral acquires the form

$$\mathscr{F}(z) = \frac{W\varepsilon}{\pi}\int_0^1 \frac{u\,du}{\sqrt{1-u^2}}\left[\cos^2(u\varepsilon L) + \frac{\sin^2(u\varepsilon L)}{u^2} - z\right]^{-1}. \tag{16}$$

Trigonometric functions in the integrand rapidly oscillate. To take advantage of this property, we represent the integrand as a sum over Fourier harmonics $\cos(nu\varepsilon L)$. The first and the second terms of such Fourier expansion are

$$\mathscr{F}(z) = \frac{W\varepsilon}{\pi\sqrt{1-z}}\int_0^1 \frac{u^2\,du}{\sqrt{(1-u^2)(1-zu^2)}}\left[1 + \frac{2\left(u\sqrt{1-z} - \sqrt{1-zu^2}\right)^2}{1-u^2}\cos(2u\varepsilon L)\right]. \tag{17}$$

The first term of the above expression provides the main (linear in ε) contribution to the generating function. It is expressed in terms of complete elliptic integrals. The second term is suppressed due to oscillations of the integrand. We estimate its contribution using the saddle-point method. The result of this calculation reads

$$\mathscr{F}(z) = W\varepsilon\left[\frac{K(z) - E(z)}{\pi z\sqrt{1-z}} + \frac{\sin(2\varepsilon L - \pi/4)}{8\sqrt{\pi}(1-z)^2(\varepsilon L)^{3/2}}\right]. \tag{18}$$

The conductance and the Fano factor are then calculated by expanding $\mathscr{F}(z)$ in small z, see Eq. (15).

$$G = \frac{e^2}{h}\,W\varepsilon\left[1 + \frac{\sin(2\varepsilon L - \pi/4)}{2\sqrt{\pi}(\varepsilon L)^{3/2}}\right], \tag{19}$$

$$F = \frac{1}{8}\left[1 - \frac{9\sin(2\varepsilon L - \pi/4)}{2\sqrt{\pi}(\varepsilon L)^{3/2}}\right]. \tag{20}$$

These results are in a good agreement with the high-energy behavior of G and F calculated numerically, see Fig. 2.

Let us emphasize that transport properties of the system at high energies depend on the particular model of the contacts [40, 41]. In our calculation we assume that the boundaries between graphene and the leads are sharp. This model is well justified if the actual extension d of the transitional region at the interface is small compared to the electron wavelength in graphene. This condition is violated at very high energy, $\varepsilon \gg 1/d$, when the boundary becomes adiabatically smooth. This, in particular, leads to the vanishing Fano factor because the semiclassically propagating electrons are either transmitted or reflected without any uncertainty.

Our results for the energy dependence of the conductance and the Fano factor in clean graphene are in agreement with the findings of Refs. [16, 38], where the sum over transmission channels was evaluated numerically for a finite (but sufficiently large) ratio W/L. Experimentally, such a ballistic setup was studied in Refs. [19, 20]. Most of the experimental observations reasonably agree with our results. The "conductivity" GL/W (which is equal to $4e^2/\pi h$ at the neutrality point, as expected for a ballistic sample) increases roughly linearly with energy ε. The Fano factor has a value close to $1/3$ at the Dirac point and decreases when one moves away from the Dirac point, showing a tendency to saturate at $F \approx 0.15$, which is not far from the value 1/8 we have obtained in the high-energy regime. Measurements on other samples reveal that very far from the Dirac point the Fano factor decreases again, reaching a value as low as 0.02. Apparently, the intermediate plateau corresponds to the high-energy regime $L^{-1} \ll \varepsilon \ll d^{-1}$ investigated in our work, while the vanishing of the Fano factor at still higher electron concentrations corresponds to the ultra-high-energy range, $\varepsilon \gg d^{-1}$.

4. INCLUDING DISORDER: PERTURBATIVE TREATMENT

So far, we have considered the transport properties of a clean graphene sample. In the present section we include disorder on the level of the leading perturbative correction. We assume the Gaussian statistics for the random potential $V(x,y)$,

$$\begin{gathered}\langle V(x,y)\rangle = 0,\\ \langle V(x,y)V(x',y')\rangle = 2\pi\alpha\delta(x-x')\delta(y-y').\end{gathered} \tag{21}$$

The dimensionless disorder strength α is similar to the parameter α_0 used in Ref. [30].

The Gaussian white-noise disorder (21) is realized when the scattering is due to impurities in the substrate separated by a thick (compared to the lattice constant) clean spacer layer from the graphene plane. The intervalley matrix elements of the disorder potential are then exponentially suppressed and can be safely neglected. A more realistic case of long-range charged impurities with $1/r$ potentials can also be treated perturbatively within the Gaussian model, but with an energy-dependent scattering amplitude [29].

In the present section we will calculate the first disorder correction to the transport properties of a graphene sample. Specifically, we will find a linear-in-α contribution to the distribution function $P(T)$ at low energies and to the generating function $\mathscr{F}(z)$ at high energies.

4.1. Low energies: $\varepsilon L \ll 1$

We have already calculated the lowest order correction to the distribution function $P(T)$ due to small energy [see Eq. (11)]. Now we are going to find the lowest disorder correction at exactly zero energy. To the main order, these two contributions merely add up.

At zero energy, there are no propagating modes in graphene, all the channels are evanescent. The generating function $\mathscr{F}(z)$ defined by Eq. (15) at $\varepsilon = 0$ simplifies to

$$\mathscr{F}_0(z) = \frac{W}{2\pi L}\int \frac{dp}{\cosh^2 p - z} = \frac{W}{\pi L}\,\frac{\arcsin\sqrt{z}}{\sqrt{z-z^2}}. \tag{22}$$

In order to find the lowest disorder correction to the generating function, we solve the evolution equation (6) perturbatively up to second order in random potential. Then we single out the transmission matrix t from $\mathscr{T}$ and substitute it into Eq. (15). After averaging over Gaussian distribution (21) the correction to the generating function acquires the form

$$\mathscr{F}_{\rm dis}(z) = \frac{2\alpha W}{\pi L}\,\frac{\arcsin\sqrt{z}}{\sqrt{z-z^2}}. \tag{23}$$

Remarkably, the disorder correction retains the functional form of $\mathscr{F}(z)$ at zero energy changing only the overall prefactor. We will discuss the consequences of this fact in Sec. 6. This implies that the transmission distribution $P(T)$ also preserves its Dorokhov form. Together with the energy correction from Eq. (11), we find the following result

$$P(T) = \frac{W}{2\pi L}\,\frac{1}{T\sqrt{1-T}}\left[1+2\alpha + (\varepsilon L)^2\left(\frac{\sqrt{1-T}}{\operatorname{arccosh}^3\frac{1}{\sqrt{T}}} - \frac{1+T}{2\operatorname{arccosh}^2\frac{1}{\sqrt{T}}}\right)\right]. \tag{24}$$

4.2. High energies: $\varepsilon L \gg 1$

The transport properties of a clean graphene sample at high energies were considered in Sec. 3.2. The main contribution to the conductance and to higher moments is proportional to εL and comes from the band of fully opened channels with $|p_n| < \varepsilon$. Carrying out the same perturbative calculation as for the zero-energy case, we get a complicated double integral of a rapidly oscillating function. After averaging over oscillations, the integral simplifies and yields the disorder correction to the generating function

$$\mathscr{F}_{\rm dis}(z) = -\alpha W L \varepsilon^2 \frac{[(1-z)K(z) - E(z)]^2}{\pi z^2 (1-z)}. \qquad (25)$$

Expanding at $z = 0$, we readily calculate disorder corrections to the conductance and Fano factor. Combining these corrections with the results for clean sample, Eqs. (19) and (20), we obtain

$$G = \frac{e^2}{h} W\varepsilon \left[1 + \frac{\sin(2\varepsilon L - \pi/4)}{2\sqrt{\pi}(\varepsilon L)^{3/2}} - \frac{\pi}{4}\alpha\varepsilon L\right], \qquad (26)$$

$$F = \frac{1}{8}\left[1 - \frac{9\sin(2\varepsilon L - \pi/4)}{2\sqrt{\pi}(\varepsilon L)^{3/2}} + \frac{3\pi}{4}\alpha\varepsilon L\right]. \qquad (27)$$

We see that at high energies any disorder suppresses conductance and enhances noise at the level of the lowest perturbative correction.

At sufficiently high energies, $\alpha\varepsilon L \gtrsim 1$, disorder correction becomes comparable to the clean result. This implies a crossover to the diffusive regime, where the perturbative approach developed in the present section fails, see Sec. 5.

5. RENORMALIZATION GROUP AND OVERALL PHASE DIAGRAM

In the previous section we have calculated the lowest disorder correction to transport properties of a ballistic graphene sample. In the present section we will discuss the resummation of higher-order contributions.

The second-order and all higher terms contain logarithmic divergences and thus become important when system is still in the ballistic regime, $L \ll l$. These logarithms are intrinsic for two-dimensional Dirac fermions subjected to disorder and were extensively studied in various contexts using renormalization group technique. [42, 43, 44, 45, 46, 47] Application of such a renormalization group (RG) to disordered graphene was developed in Refs. [48, 29].

We will use two-loop perturbative RG for the disorder strength α and one-loop for the energy ε. Higher terms in the RG equations are non-universal and depend on the particular regularization scheme. A comprehensive derivation of the two-loop RG equations can be found in, e.g., Ref. [49].

$$\frac{\partial\alpha}{\partial\ln\Lambda} = 2\alpha^2 + 2\alpha^3, \qquad \frac{\partial\varepsilon}{\partial\ln\Lambda} = \alpha\varepsilon. \qquad (28)$$

Here Λ is the running scale parameter in the real space, it has the dimension of length. Bare values of energy and disorder coupling, which are the initial conditions for RG equations, correspond to the scale of the order of lattice spacing a. After renormalization procedure, we obtain renormalized values of the parameters at the scale Λ and also a new effective bandwidth $1/\Lambda$.

The renormalization proceeds until one of the following events happens: (i) the running scale Λ reaches the system size L, (ii) the disorder coupling becomes of the order unity, or (iii) the renormalized energy reaches the bandwidth. We will discuss these three possibilities below. Once the renormalization has been performed, we can calculate observables by simply applying the perturbation theory. The results of previous section for transport characteristics thus remain applicable with bare parameters replaced by their renormalized values.

Let us first consider the zero energy limit when the only parameter of the model is the disorder strength α. Disorder is enhanced in course of renormalization. The RG should be stopped when the renormalized value of α becomes of order of unity, so that the perturbative expansion of the beta function fails. The corresponding scale is the zero-energy mean free path

$$l_0 = a\sqrt{\alpha}e^{1/2\alpha}. \qquad (29)$$

At scales shorter than the mean free path l_0, the renormalized value of α is given by

$$\alpha(\Lambda) = \frac{1}{2\ln(l_0/\Lambda) + \ln\ln(l_0/\Lambda)}. \qquad (30)$$

As long as $L \ll l_0$, and thus $\alpha(L) \ll 1$, we can describe the transport properties by the distribution function (24) with the renormalized value $\alpha(L)$ and $\varepsilon = 0$.

A small but non-zero energy does not change the qualitative behavior of the system, as long as the RG flow is terminated by the system size. We refer to this situation as "ultraballistic regime". The energy gets renormalized according to Eq. (28),

$$\varepsilon(\Lambda) = \frac{\varepsilon}{\sqrt{\alpha[2\ln(l_0/\Lambda) + \ln\ln(l_0/\Lambda)]}}. \qquad (31)$$

The value $\varepsilon(L)$ is to be substituted into Eq. (24) along with the renormalized value of $\alpha(L)$. This yields the full description of transport properties for the system in the ultraballistic regime. In particular, the conductance and

the Fano factor are

$$G = \frac{4e^2}{\pi h}\,\frac{W}{L}\left[1+\frac{2\alpha + c_1(\varepsilon L)^2}{\alpha[2\ln(l_0/L)+\ln\ln(l_0/L)]}\right], \quad (32)$$

$$F = \frac{1}{3}\left[1+\frac{c_2(\varepsilon L)^2}{\alpha[2\ln(l_0/L)+\ln\ln(l_0/L)]}\right], \quad (33)$$

with the constants $c_{1,2}$ given by Eqs. (13) and (14).

When the initial (bare) value of energy is increased, the renormalized energy eventually becomes comparable to the effective bandwidth $1/\Lambda$ before the running scale Λ reaches L (and still before the disorder coupling $\alpha(\Lambda)$ reaches unity). The length scale at which $\varepsilon(\Lambda) = 1/\Lambda$ plays the role of the effective Fermi wavelength λ. (Indeed, in the absence of disorder, energy is not renormalized and $\lambda = 1/\varepsilon$.) Using Eq. (31), we find

$$\lambda = \frac{1}{\varepsilon}\sqrt{2\alpha\ln(\varepsilon/\gamma)}, \quad (34)$$

where γ is the characteristic disorder-induced energy scale

$$\gamma = \sqrt{\alpha}/l_0 = \Delta e^{-1/2\alpha}, \quad (35)$$

$\Delta = 1/a$ is the initial bandwidth of the model, and we assumed that $\varepsilon \gg \gamma$. According to Eqs. (30) and (34), the renormalized value of the coupling constant at the scale of the Fermi wave length is

$$\alpha(\lambda) = \frac{1}{2\ln(\varepsilon/\gamma)}. \quad (36)$$

In Fig. 3 we show the phase diagram of various transport regimes. If $\varepsilon \lesssim \gamma$ and $L \ll l_0$ or, alternatively, $\varepsilon \gtrsim \gamma$ and $L \ll \lambda$, the renormalization terminates by the system size, $\Lambda = L$, and the system is in the ultraballistic regime discussed above [see Eqs. (32) and (33)]. If $\varepsilon \gg \gamma$ and $\lambda \ll L \ll l$, the renormalization stops at $\Lambda = \lambda$ and the running scale does not reach L. We refer to this case as "ballistic regime", since the system size is still smaller than the mean free path l,

$$l = \frac{\lambda}{\pi\alpha(\lambda)} = \frac{\sqrt{\alpha}}{\pi\varepsilon}[2\ln(\varepsilon/\gamma)]^{3/2}. \quad (37)$$

This value [29] of the mean free path is a result of the standard Born approximation with renormalized coupling constant $\alpha(\lambda)$. Note that for the model with random scalar potential, the transport mean free path, which determines diffusion coefficient, is twice longer, $l_{\rm tr} = 2l$.

In the ballistic regime, the renormalized energy is such that $\varepsilon(\lambda)L = L/\lambda \gg 1$. This means that we have to use the high-energy results of Sec. 4.2. In particular, with the renormalized parameters, the conductance and the Fano factor, Eqs. (26) and (27), become

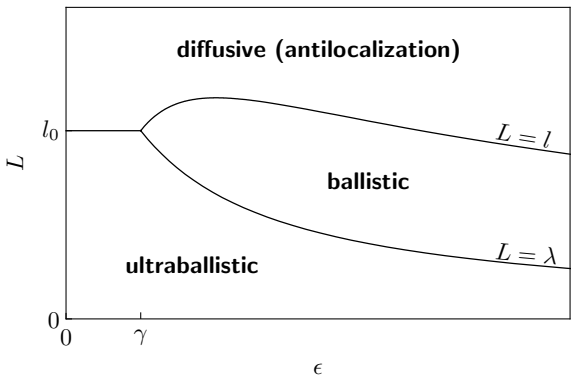

FIGURE 3. Schematic "phase diagram" of various transport regimes in the graphene sample with random potential. The lines indicate crossovers between corresponding regimes. The shortest sample exhibits ultraballistic transport with the conductance and Fano factor given by Eqs. (32) and (33) respectively. When the length of the sample exceeds Fermi wave length (34), ballistic results (38) and (39) apply. In a sample longer than the mean free path (37), diffusive regime establishes with the Drude conductivity (40) and the Dorokhov distribution of transmission eigenvalues (41). The conductivity experiences symplectic antilocalization in this case.

$$G = \frac{e^2}{h}\,\frac{W}{\lambda}\left[1+\frac{\sin(2L/\lambda-\pi/4)}{2\sqrt{\pi}(L/\lambda)^{3/2}}-\frac{L}{4l}\right], \quad (38)$$

$$F = \frac{1}{8}\left[1-\frac{9\sin(2L/\lambda-\pi/4)}{2\sqrt{\pi}(L/\lambda)^{3/2}}+\frac{3L}{4l}\right]. \quad (39)$$

In the expressions (38) and (39) there are two corrections to the leading term. The first (oscillating) correction exists in the clean limit and is small provided $L \gg \lambda$. The second correction due to disorder is small only if $L \ll l$. This imposes the natural upper bound on the ballistic regime: if the system size exceeds the mean free path, electron transport becomes diffusive. In this case, the system is naturally characterized by the conductivity σ, which determines the conductance via the Ohm's law, $G = \sigma W/L$. The Drude expression for the conductivity reads [48]

$$\sigma = \frac{4e^2}{\pi h\alpha(\lambda)} = \frac{8e^2}{\pi h}\ln(\varepsilon/\gamma). \quad (40)$$

The distribution function of transmission eigenvalues in the diffusive regime is the same as in a usual quasi-one-dimensional metallic sample [39]

$$P(T) = \frac{W}{2\pi L}\,\frac{g}{T\sqrt{1-T}}, \quad (41)$$

with the dimensionless conductivity $g = (\pi h/4e^2)\sigma$. Taking into account interference effects leads to L dependence of g in this formula, as we are going to discuss.

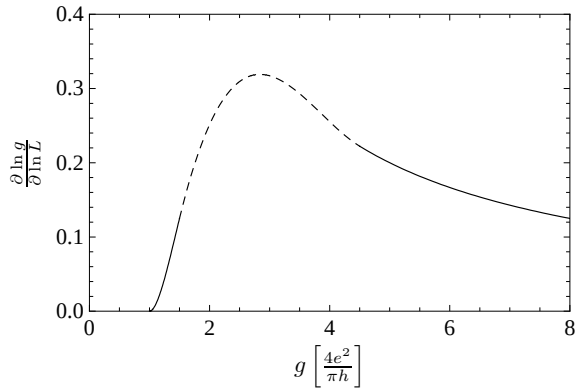

FIGURE 4. Unified scaling function (43) for both ultraballistic and diffusive regimes at zero energy in the case of the random potential disorder.

6. SINGLE PARAMETER SCALING AT ZERO ENERGY

Remarkably, the transmission distribution function at zero energy appears to be the same in ultraballistic and diffusive limits. In both cases it has the form of Dorokhov distribution (41) with the parameter

$$g = \begin{cases} 1+2\alpha(L), & \text{ultraballistic}, \\ \dfrac{\pi h}{4e^2}\,\sigma(L), & \text{diffusive}, \end{cases} \tag{42}$$

which has the meaning of the dimensionless conductivity. In the ultraballistic regime, the scaling of g is induced via renormalization of α according to equation (28) while in the diffusive limit, $g \gg 1$ acquires antilocalization corrections characteristic for a disordered system of symplectic symmetry. This allows us to infer a unified scaling law covering both limiting cases

$$\frac{\partial \ln g}{\partial \ln L} = \begin{cases} (g-1)^2 - (g-1)^3/2, & g-1 \ll 1, \\ 1/g, & g \gg 1. \end{cases} \tag{43}$$

The scaling function (43) is depicted in Fig. 4. It is qualitatively similar to the numerical results of Ref. [10].

We stress that the ultraballistic asymptotics of the beta function in Eq. (43) is only valid for Gaussian white-noise statistics of random potential. The interpolation between the two asymptotics of the beta function in Fig. 4 implicitly assumes a smooth crossover between the two regimes (in particular, without any intermediate fixed points), as suggested by numerical simulations. [10, 11, 12, 14]

The scaling function (43) characterizes the evolution of the dimensionless conductivity with increasing L. Whether the full distribution function $P(T)$ retains exactly its form (41) (parameterized by g only) in the crossover remains an open question. Strictly speaking, what we know at the moment is that this form of $P(T)$ emerges (i) in the clean limit, (ii) in the ultraballistic regime within the first order in $\alpha(L)$, and (iii) in the diffusive regime. On this basis, one could speculate that this might be an exact statement for the whole crossover.

7. SUMMARY

In this paper, we have analyzed transport properties of a graphene sample in the "wide and short" geometry, $W \gg L$, with disorder effects restricted to a random potential scattering within a single valley. Starting from the clean limit and using the transfer-matrix technique, we have analyzed the evolution of the transmission distribution $P(T)$ and, in particular, of the conductance G and the Fano factor F, with increasing system size L. To take the randomness into account, we have developed a perturbative treatment of the transfer-matrix equations supplemented by an RG formalism describing the renormalization of disorder couplings. This has allowed us to get complete analytical description of the transport properties of graphene in the ultraballistic ($L \ll \lambda$) and ballistic ($\lambda \ll L \ll l$) regimes. We have also constructed "phase diagrams" of different transport regimes (ultraballistic, ballistic, diffusive).

ACKNOWLEDGMENTS

We are grateful to M. Titov, A.W.W. Ludwig, P. San-Jose, E. Prada, and H. Schomerus for valuable discussions. The work was supported by the Center for Functional Nanostructures of the Deutsche Forschungsgemeinschaft. The work of I.V.G. was supported by the EUROHORCS/ESF EURYI Awards scheme. I.V.G. and A.D.M. acknowledge kind hospitality of the Isaac Newton Institute for Mathematical Sciences of the Cambridge University during the program "Mathematics and physics of Anderson localization: 50 years after", where a part of this work was performed.

REFERENCES

1. K.S. Novoselov, A.K. Geim, S.V. Morozov, D. Jiang, Y. Zhang, S.V. Dubonos, I.V. Grigorieva, and A.A. Firsov, Science **306**, 666 (2004).
2. K.S. Novoselov, D. Jiang, F. Schedin, T.J. Booth, V.V. Khotkevich, S.V. Morozov, and A.K. Geim, Proc. Natl. Acad. Sci. U.S.A. **102**, 10451 (2005).
3. K.S. Novoselov, A.K. Geim, S.V. Morozov, D. Jiang, M.I. Katsnelson, I.V. Grigorieva, S.V. Dubonos, and A.A. Firsov, Nature (London) **438**, 197 (2005).

4. Y. Zhang, Y.-W. Tan, H.L. Stormer, and P. Kim, Nature (London) **438**, 201 (2005).
5. A.K. Geim and K.S. Novoselov, Nature Materials **6**, 183 (2007).
6. A.H. Castro Neto, F. Guinea, N.M.R. Peres, K.S. Novoselov, and A.K. Geim, arXiv:0709.1163, to appear in Rev. Mod. Phys.
7. Y.-W. Tan, Y. Zhang, H.L. Stormer, and P. Kim, Eur. Phys. J. Special Topics, **148**, 15 (2007).
8. K. Nomura and A.H. MacDonald, Phys. Rev. Lett. **98**, 076602 (2007).
9. A. Rycerz, J. Tworzydlo, and C.W.J. Beenakker, Europhys.Lett. **79**, 57003 (2007).
10. J.H. Bardarson, J. Tworzydło, P.W. Brouwer, and C.W.J. Beenakker, Phys. Rev. Lett. **99**, 106801 (2007).
11. K. Nomura, M. Koshino, and S. Ryu, Phys. Rev. Lett. **99**, 146806 (2007).
12. P. San-Jose, E. Prada, and D.S. Golubev, Phys. Rev. B **76**, 195445 (2007).
13. C.H. Lewenkopf, E.R. Mucciolo, and A.H. Castro Neto, Phys. Rev. B **77**, 081410R (2008).
14. J. Tworzydlo, C.W. Groth, and C.W.J. Beenakker, arXiv:0810.4787.
15. M.I. Katsnelson, Eur. Phys. J. B **51**, 157 (2006).
16. J. Tworzydlo, B. Trauzettel, M. Titov, A. Rycerz, and C.W.J. Beenakker, Phys. Rev. Lett. **96**, 246802 (2006).
17. H.B. Heersche, P. Jarillo-Herrero, J.B. Oostinga, L.M.K. Vandersypen, and A.F. Morpurgo, Nature **446**, 56 (2007).
18. F. Miao, S. Wijeratne, Y. Zhang, U.C. Coskun, W. Bao, and C.N. Lau, Science **317**, 1530 (2007).
19. R. Danneau, F. Wu, M.F. Craciun, S. Russo, M.Y. Tomi, J. Salmilehto, A.F. Morpurgo, and P.J. Hakonen, Phys. Rev. Lett. **100**, 196802 (2008).
20. R. Danneau, F. Wu, M.F. Craciun, S. Russo, M.Y. Tomi, J. Salmilehto, A.F. Morpurgo, and P.J. Hakonen, arXiv:0807.0157.
21. C.W.J. Beenakker, Rev. Mod. Phys. **69**, 731 (1997).
22. S. Ryu, C. Mudry, A. Furusaki, and A.W.W. Ludwig, Phys. Rev. B **75**, 205344 (2007).
23. Some analytical results for ballistic transport in graphene were obtained within the toy-model of one-dimensional disorder in Refs. [12, 38]. In the present paper, we address the realistic case of a truly two-dimensional disorder.
24. P.M. Ostrovsky, I.V. Gornyi, and A.D. Mirlin, Phys. Rev. B **77**, 195430 (2008).
25. F.V. Tikhonenko, D.W. Horsell, R.V. Gorbachev, and A.K. Savchenko, Phys. Rev. Lett. **100**, 056802 (2008).
26. T. Ando, J. Phys. Soc. Jpn **75**, 074716 (2006).
27. K. Nomura and A.H. MacDonald, Phys. Rev. Lett. **96**, 256602 (2006).
28. D.V. Khveshchenko, Phys. Rev. B **75**, 241406(R) (2007).
29. P.M. Ostrovsky, I.V. Gornyi, and A.D. Mirlin, Phys. Rev. B **74**, 235443 (2006).
30. P.M. Ostrovsky, I.V. Gornyi, and A.D. Mirlin, Phys. Rev. Lett. **98**, 256801 (2007).
31. P.M. Ostrovsky, I.V. Gornyi, and A.D. Mirlin, Eur. Phys. J. Special Topics **148**, 63 (2007).
32. S. Ryu, C. Mudry, H. Obuse, and A. Furusaki, Phys. Rev. Lett. **99**, 116601 (2007).
33. D. Hsieh, D. Qian, L. Wray, Y. Xia, Y. Hor, R.J. Cava and M.Z. Hasan Nature **452**, 970 (2008).
34. A.P. Schnyder, S. Ryu, A. Furusaki, and A.W.W. Ludwig, arXiv:0803.2786
35. A. Schuessler, P.M. Ostrovsky, I.V. Gornyi, and A.D. Mirlin, arXiv:0809.3782.
36. M. Titov and C.W.J. Beenakker, Phys. Rev. B **74**, 041401(R) (2006).
37. V.V. Cheianov and V.I. Fal'ko, Phys. Rev. B **74**, 041403 (2006).
38. M. Titov, Europhys. Lett. **79**, 17004 (2007).
39. O.N. Dorokhov, Zh. Eksp. Teor. Fiz. **85**, 1040 (1983) [Sov. Phys. JETP **58**, 606 (1983)].
40. H. Schomerus, Phys. Rev. B **76**, 045433 (2007).
41. Ya.M. Blanter and I. Martin, Phys. Rev. B **76**, 155433 (2007).
42. V.S. Dotsenko and V.S. Dotsenko, Adv. Phys. **32**, 129 (1983).
43. A.W.W. Ludwig, M.P.A. Fisher, R. Shankar, and G. Grinstein, Phys. Rev. B **50**, 7526 (1994);
44. A. A. Nersesyan, A. M. Tsvelik, and F. Wenger, Phys. Rev. Lett. **72**, 2628 (1994); Nucl. Phys. B **438**, 561 (1995).
45. M. Bocquet, D. Serban, and M.R. Zirnbauer, Nucl. Phys. B **578**,628 (2000).
46. A. Altland, B.D. Simons, and M.R. Zirnbauer, Phys. Rep. **359**, 283 (2002).
47. S. Guruswamy, A. LeClair, and A.W.W. Ludwig, Nucl. Phys. B **583**, 475 (2000).
48. I.L. Aleiner and K.B. Efetov, Phys. Rev. Lett. **97**, 236801 (2006).
49. A. Bondi, G. Curci, G. Pattuti, and P. Rossi, Ann. Phys. **199**, 268 (1990).